Nuclear Engineering and Technology 55 (2023) 2315–2324

Contents lists available at ScienceDirect

Nuclear Engineering and Technology

journal homepage: www.elsevier.com/locate/net

Original Article

Conceptual design of a dual drum-controlled space molten salt reactor (D^2-SMSR): Neutron physics and thermal hydraulics

Yongnian Song [a], Nailiang Zhuang [a, b, *], Hangbin Zhao [b, c], Chen Ji [d], Haoyue Deng [d], Xiaobin Tang [a, b, **]

[a] Department of Nuclear Science and Technology, Nanjing University of Aeronautics and Astronautics, Nanjing, 211106, China
[b] Key Laboratory of Nuclear Technology Application and Radiation Protection in Astronautics, Ministry of Industry and Information Technology, Nanjing, 211106, China
[c] College of Astronautics, Nanjing University of Aeronautics and Astronautics, Nanjing, 211106, China
[d] State Key Laboratory of Space Power-sources Technology, Shanghai Institute of Space Power-Sources, 2965 Dongchuan Road, Shanghai, 200245, China

ARTICLE INFO

Article history:
Received 28 September 2022
Received in revised form
19 February 2023
Accepted 6 March 2023
Available online 10 March 2023

Keywords:
Space nuclear reactor
Molten salt reactor
Safety drums
Neutron physics
Thermal-hydraulic

ABSTRACT

Space nuclear reactors are becoming popular in deep space exploration owing to their advantages of high-power density and stability. Following the fourth-generation nuclear reactor technology, a conceptual design of the dual drum-controlled space molten salt reactor (D^2-SMSR) is proposed. The reactor concept uses molten salt as fuel and heat pipes for cooling. A new reactivity control strategy that combines control drums and safety drums was adopted. Critical physical characteristics such as neutron energy spectrum, neutron flux distribution, power distribution and burnup depth were calculated. Flow and heat transfer characteristics such as natural convection, velocity and temperature distribution of the D^2-SMSR under low gravity conditions were analyzed. The reactivity control effect of the dual-drums strategy was evaluated. Results showed that the D^2-SMSR with a fast spectrum could operate for 10 years at the full power of 40 kWth. The D^2-SMSR has a high heat transfer coefficient between molten salt and heat pipe, which means that the core has a good heat-exchange performance. The new reactivity control strategy can achieve shutdown with one safety drum or three control drums, ensuring high-security standards. The present study can provide a theoretical reference for the design of space nuclear reactors.

1. Introduction

With the realization of the landing on the moon and Mars, the base construction of the star catalog will be implemented in a matter of time [1]. Knowing how to realize a long-term and stable supply of energy is one of the important issues in the base construction of the star catalog. At present, solar energy is the most widely used energy in space missions. However, solar energy always needs sunlight, and it cannot work normally at night-side or in far-reaching spaces where solar energy decays violently [2]. Usually, chemical energy is used at the launch and propulsion of spacecraft, but it can only operate in the earth's atmosphere or on a small scale in the space environment [3]. The isotope power supply can supply long-term energy, but it can only provide watt-level electric power [4,5]. Space nuclear reactors based on fission energy can provide long-life, stable, and high-density electricity [6]. In the near and far future, space nuclear fission energy systems will become the most preferred potential technical solution for long-term and high-power deep space missions.

Space nuclear reactors evolved from land-based nuclear reactors. Since the concept of a space nuclear reactor was proposed, many space reactor design schemes have appeared. According to the different cooling methods, space nuclear reactors mainly take the following three forms: liquid metal-cooled reactors [7–9], gas-cooled reactors [10,11], and heat pipe reactors [12–14]. However, the schemes of these reactors all use solid fuel. With the development of fourth-generation nuclear reactor technologies, the molten salt reactor has been widely investigated. Many countries have proposed different schemes for using molten salt reactors to supply

* Corresponding author. Department of Nuclear Science and Technology, Nanjing University of Aeronautics and Astronautics, Nanjing, 211106, China.
** Corresponding author. Department of Nuclear Science and Technology, Nanjing University of Aeronautics and Astronautics, Nanjing, 211106, China.
E-mail addresses: zhuangnailiang@nuaa.edu.cn (N. Zhuang), tangxiaobin@nuaa.edu.cn (X. Tang).

https://doi.org/10.1016/j.net.2023.03.011
1738-5733/

energy since the concept was proposed [15–19]. In recent years, the application of molten salt reactors in space has been gradually considered. The United States and Japan have both proposed a design scheme for the space molten salt reactor [20,21]. The research on space molten salt reactors in China has also shown an increasing trend. Li et al. [22] proposed a design scheme for molten salt reactors that combine liquid and solid fuels to attain compact structures with high-fuel consumption. Cui et al. [23] proposed a micro-space molten salt reactor scheme requiring 50 kWth, with a high negative feedback coefficient. Yu et al. [24] proposed the M^2SR-1 scheme, in which the upper part of the core is cylindrical and the lower part is hemispherical to reduce the fuel salt load. The molten salt reactor is capable of producing high temperatures under atmospheric conditions, has high stability, and is highly safe [25–28]. In this regard, the molten salt reactor is a suitable reactor type for space nuclear reactors.

Control systems are the central components used to ensure the safety of space nuclear reactors. The three main components in a space nuclear reactor's existing reactivity control strategy are control rods, control drums, and sliding reflectors. Control rods increase the axial size of the core. When inserted into the core, control rods affect the power distribution and harm the power output [11]. Sliding reflectors adjust neutron leakage to control reactivity [29]. Control drums do not disturb the core's axial power distribution. Despite this configuration, control drums have a low level of reactivity [30]. When a reactor is shut down, multiple control drums must rotate simultaneously. In an emergency shutdown, the reactivity is difficult to control using control drums. Some scholars have proposed a hybrid safety rods and control drums system [29] to solve the problem of reactor shutdown during an accident. The size of the reactor axially would be increased by safety rods that act as shutdowns in an accident. In addition, a strategy of accident-tolerant control drums [31] has been proposed to increase the worth of control drums and improve reactor safety. However, accident-tolerant control drums tend to greatly disturb the neutron flux and power in the core, which is detrimental to the core's ability to produce power. Thus, a new reactivity control is imperative.

This study presents a dual drum-controlled space molten salt reactor (D^2-SMSR) with 40 kWth output, heat pipes to cool the core, and control drums and safety drums to control the reactor's reactivity. The neutrons and thermal hydraulics of D^2-SMSR can be specified via the Monte Carlo method and finite element simulation. The rest of this paper is organized as follows. In Section 2, the structure of the D^2-SMSR is described. In Section 3, the simulation and calculation methods are introduced. In Section 4.1, the neutron spectrum, flux distributions and depletion are presented. In Section 4.2, the flow and heat transfer characteristics of the molten salt in D^2-SMSR are analyzed. In Section 4.3, the reactivity control performance and safety of control drums failure are discussed. Finally, a summary is given in Section 5. This research can provide theoretical support for the design and development of space nuclear reactors.

2. Structure design of D^2-SMSR

Given the advantages of the molten salt reactor, its use in space has also become a promising endeavor. For D^2-SMSR, efficient and passive heat pipes are preferred for heat transfer, and the fuel salt should be stored in the reactor vessel [32]. Since the control rod affects the axial dimension, the D^2-SMSR uses the control drum as the control mechanism to make the core compact. Two kinds of control drums are used in the D^2-SMSR to improve accident safety. As accident-tolerant control drums are larger than control drums in size, and part of the fuel is away from the core when rotating, they have a higher worth of reactivity than control drums. They can be applied during an emergency shutdown. Thus, the accident-tolerant control drums serve as safety drums. By contrast, traditional control drums are used for regulating reactivity.

The core structure of the proposed D^2-SMSR is shown in Fig. 1, and the main parameters are shown in Table 1. The main fuel salt region and the safety drum fuel region form a cylinder with a diameter of 30.6 cm and a height of 30.6 cm. The nickel-based alloy with a thickness of 0.5 cm surrounds the cylinder. A total of 19 sodium heat pipes with an outside diameter of 2.4 cm are arranged in the main fuel salt region. From the outside to the inside, the heat pipes are divided into three layers, each located in a concentric circle with the core at its center. Heat pipes are spaced 6.12 cm apart between adjacent layers, and the outermost heat pipe is located 3.06 cm from the main fuel salt region's edge. The hot end of the heat pipe is connected to the core, and the cold end is connected to the thermoelectric device. Heat pipe working fluid is vaporized in the core, cooled, and liquefied at the end of the thermoelectric device. It circulates through capillary force. This way, the heat pipe can complete the heat transfer by relying on the phase change absorption and release of the latent heat of vaporization of the internal liquid working medium. The composition of the fuel is LiF-UF_4, the enrichment of ^{235}U is 93%, and the abundance of ^7Li is 99.9% [33]. A reflector with a thickness of 12 cm is arranged between the inner and outer alloys, and the material is BeO. Four control drums and two safety drums are embedded in the reflector and symmetrically arranged. The control drum is composed of reflector material and a neutron absorber with a cladding angle of 120° and a thickness of 0.5 cm. The control drum can rotate around its central axis and adjust the reactivity by changing the position of the absorber. Besides the materials in the control drums, the safety drums also contain fuel salt. As the safety drum fuel region can be coupled with the main fuel salt region, a cylindrical structure can be formed.

Reactivity control is realized by control drums and safety drums. As is shown in Fig. 2, when D^2-SMSR is working, safety drums keep still and control drums rotate to adjust the reactivity and compensate for the reactivity change of fuel due to temperature change and burn-up. If an emergency shutdown is required under accident conditions, the reactivity can be rapidly reduced and subcritical can be reached by rotating safety drums.

3. Numerical simulation method

The neutron physical simulation method and the thermal-hydraulic simulation method are discussed in this section. Neutron physics calculations and dual-drums worth analysis of D^2-SMSR are performed via the Monte Carlo method. Thermal hydraulic calculations are conducted via the finite element method.

3.1. Neutron physical simulation method

The physical modeling and critical calculation of the D^2-SMSR are completed using MCNP 6. In critical analysis, 50000 input particles for 650 active cycles are preceded by 50 inactive cycles. The absorbers of control drums and safety drums are all distributed outwards. The value of k_{eff} is obtained at an operating temperature of 1000 K. The calculation error is approximately 0.00012. The Reactor Monte Carlo (RMC) code is used to analyze the burnup parameters and the lifetime of the D^2-SMSR. Chebyshev Rational Approximate Method is adopted to solve depletion equations [34]. The main fuel region and the safety drum fuel region are taken as the depletion zones. The power is 40 kWth, and the time step is defined as one year in the burnup calculation.

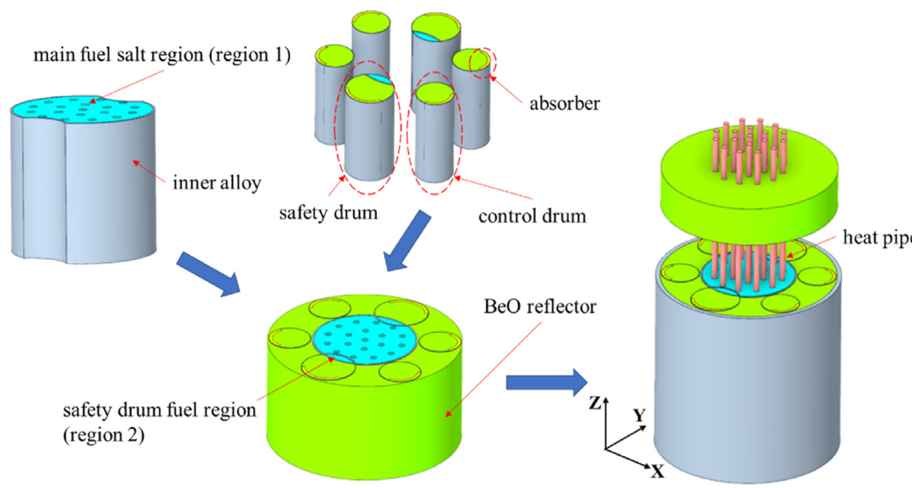

Fig. 1. 3D sketch of the core structure.

Table 1
Main parameters of D^2-SMSR.

Name	Parameter	Density /g·cm^{-3}
Thermal power/kWth	40	-
Life/year	10	-
Fuel	LiF-UF_4 (72.5%: 27.5%)	6.20-1.37*T/1000
Heat pipe	Sodium	-
Structural material	N10083 alloy	8.86
Material of reflector	BeO	3.01
Absorber material	B_4C	2.51
Control drum diameter/cm	10	-
Safety drum diameter/cm	14	-

3.2. Thermal hydraulic simulation method

The thermal calculation of the reactor is completed by ANSYS Fluent. Based on the symmetry of the core structure, a quarter of the reactor core is selected for computational analysis. This reactor core consists of three parts: the molten salt fuel in the safety drum, the fuel in the main fuel region, and the alloy. The grid is generated by Fluent Meshing, as shown in Fig. 3. A polyhedral grid is used on the surface, and a hexahedral grid is used in the core. In the thermal calculation, the choice of turbulence models is the standard k-ε model, and the enhanced wall function is built to deal with the near-wall flow. The fuel salt density and thermal expansion rate are determined based on the Boussinesq hypothesis [35]. The heat source represents the whole fission area of the reactor, and heat is considered to be evenly distributed in the fission area. The heat pipes serve as cold sources, simplified as constant temperature walls. Convergence is considered when the average temperature of the system and the residuals of all variables are stable.

4. Results and discussion

This section analyzes the critical characteristics of D^2-SMSR. In the analysis of the physical characteristics, the differences in neutron spectrum and neutron flux distribution between region 1 and region 2 are compared. The thermal-hydraulic study analyzes the heat transfer characteristics of molten salt flow in the reactor core under the Martian gravity condition. The heat transfer in the D^2-SMSR is elaborated concerning the two different heat pipe insertion depths. In the dual drum worth analysis, the influence of temperature and control drum rotation on reactivity is evaluated. In addition, whether the reactor can shut down generally under the failure of specific control drums is determined.

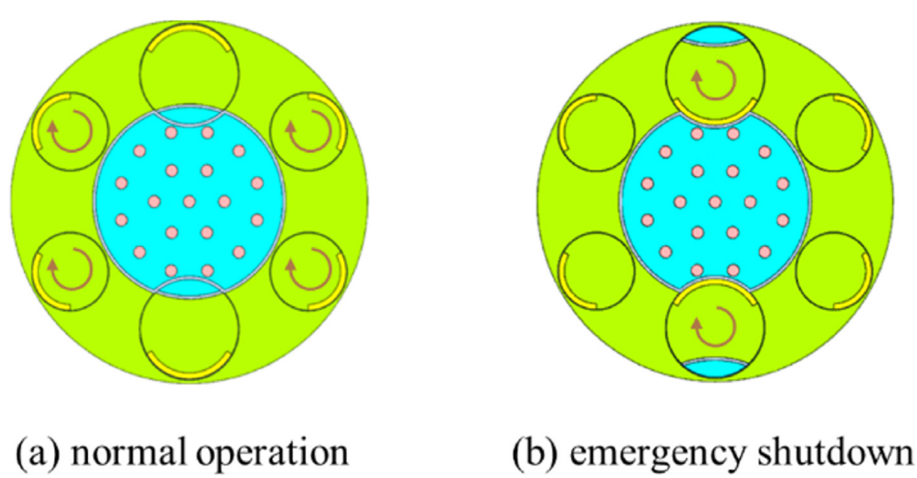

Fig. 2. Operation of control mechanism.

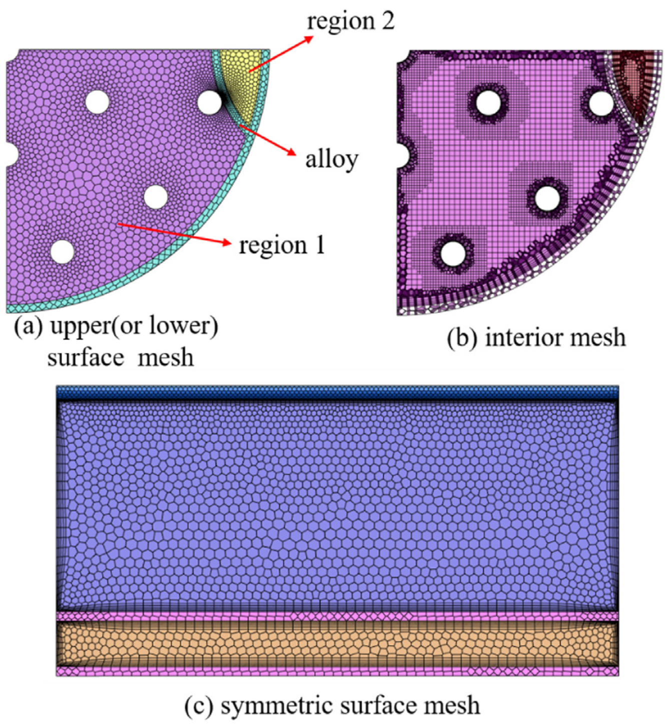

Fig. 3. Grid model of D^2-SMSR core.

4.1. Physical analysis of D^2-SMSR

4.1.1. Neutron energy spectral distribution

The neutron spectrum of the core is shown in Fig. 4. In the D^2-SMSR, most of the energy of the neutron is higher than 1 keV. Compared with region 2, there are more fast neutrons and fewer slow neutrons in region 1. More affected by the reflector, the moderation effect in region 2 is more potent than in region 1, leading to a more significant proportion of slow neutrons.

4.1.2. Neutron flux distribution

The neutron flux density in the core is calculated by the FMESH card, a mesh tally code in MCNP 6. The tally grid density is 99 × 99 × 99. The neutron flux of the cross and longitudinal sections is shown in Fig. 5. The neutron flux in the active area is roughly symmetrical and decreases from the center to the edge. The

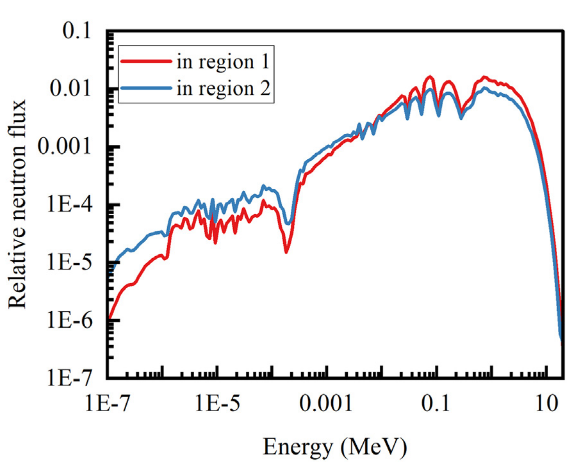

Fig. 4. Neutron distribution in different energy segments.

safety drum inserted into the core has a negligible influence on the neutron flux in the fuel area.

Fig. 6 shows the neutron flux curves of the different energy segments and radial positions. Within a 12 cm radius of the fission region, the flux distributions of the neutrons above 1 keV are essentially the same at all three locations. Region 2 has a lower neutron flux than region 1 at distances of more than 12 cm. The maximum reduction is 5.5%. This finding can be attributed to the absorption of neutrons by the alloy wrapped around safety drums. The difference in neutron flux is similar for energies below 1 eV in the fission area. On the one hand, neutron leakage in the core is lessened owing to the reflection of the BeO reflector. On the other hand, the neutron-slowing ability of BeO contributes to the presence of a small number of thermal neutrons in the fission region near the reflector. Thus, a peak in the slow neutrons in the reflector can be observed. Distribution of the neutron flux in different axial locations is shown in Fig. 7. The neutron flux distribution varies along the height direction of the nuclear reactor, initially increasing and then decreasing. The neutron flux differences between the center ($R = 0$) and edge ($R = 14$ cm) of the core are the greatest at $H = 0$ and the smallest near the top (or bottom) of the fuel area.

4.1.3. Thermal power distribution

Fig. 8 shows the power distribution at the bottom, middle, and top of the D^2-SMSR. The thermal power is more significant in the middle than at the edge. The power density curves along the axial direction are obtained to examine the power changes in region 1 and region 2. A summary of the results is shown in Fig. 9. A peak in the middle of the core decreases along the edge but rises sharply near the border, forming two troughs. A BeO reflector moderates neutrons, resulting in more slow neutrons at the edge of the fission region. Slow neutrons are more likely to cause fission with ^{235}U than fast neutrons, causing the core edge's power to increase, hence the two minimum points. Region 2 has a lower power density than region 1. Moreover, on both sides, the difference in power distribution is apparent. As shown in Figs. 6 and 7, the neutron flux in region 2 is lower than that in region 1. Thus, the power difference at the edge is greater than the middle along the height direction.

4.1.4. Burnup analysis

The RMC program calculates the average burnup of the entire core of the D^2-SMSR. The reactor operates at the rated operating temperature with full power, and the absorbers are farthest from it. Fig. 10 shows the variations in the effective multiplication factor k_{eff} of the core versus time. The k_{eff} is greater than 1 at the end of life. This trend indicates that the reactor can run at full power for 10 years with enough excess reactivity. Fig. 11 presents the change in heavy metal nuclides in the reactor core over time. With time migration, the relative instability of ^{235}U and ^{238}U in the reactor is slight, whereas the other actinide nuclides keep increasing. On the one hand, ^{235}U partially absorbs neutrons in the reactor core to generate ^{236}U, causing the most number among all other actinide nuclides. On the other hand, despite the low content, some fast neutrons in the reactor react with ^{238}U, slightly mitigating core reactivity reduction.

4.2. Thermal hydraulic analysis of D^2-SMSR

Liquid molten salt generates heat, and heat pipes are responsible for transferring heat in the molten salt space nuclear reactor. This process inevitably produces a temperature difference, leading to the natural convection of molten salt in the core. In the case of microgravity, natural convection also occurs in the molten salt reactor, changing the thermal distribution of the core. Therefore, the temperature and velocity fields are analyzed to clarify the

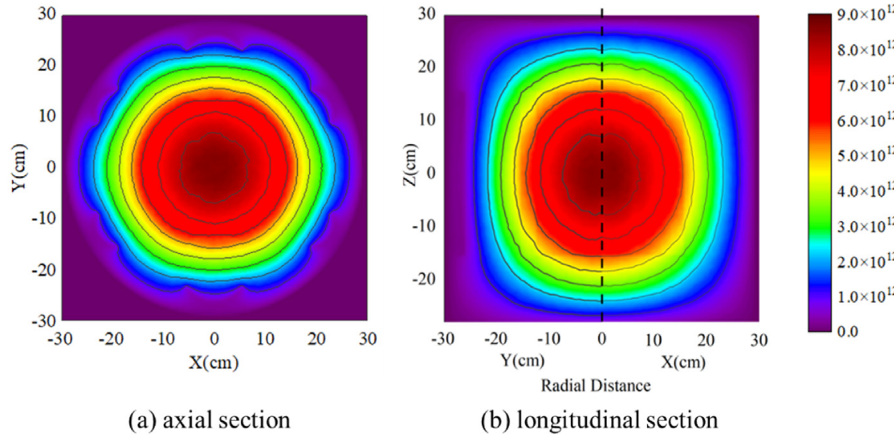

Fig. 5. Contours of neutron flux distribution (x, y and z directions are shown in Fig. 1).

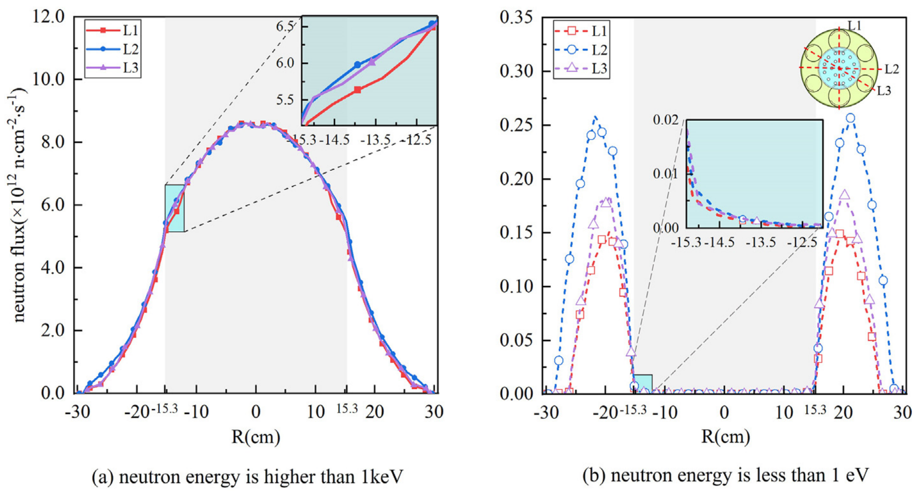

Fig. 6. Neutron flux distribution in different energy segments along radial positions(L1: the line through safety drums; L2: the line without passing safety drums and control drums; L3: the line through control drums.).

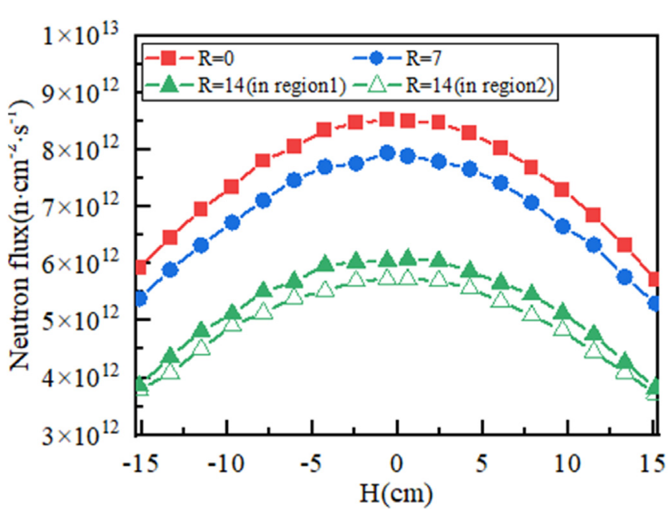

Fig. 7. Neutron flux distribution at different axial positions.

thermal change in the D^2-SMSR. Two simplified conditions of the heat pipe are considered. Condition 1 is to set the heat pipe to a constant temperature wall. Condition 2 is to set the equivalent

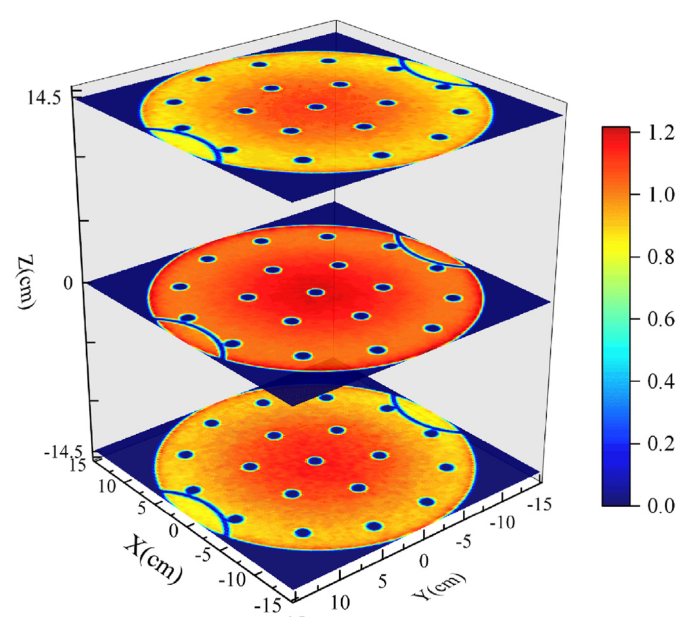

Fig. 8. Power distribution of the core at different heights.

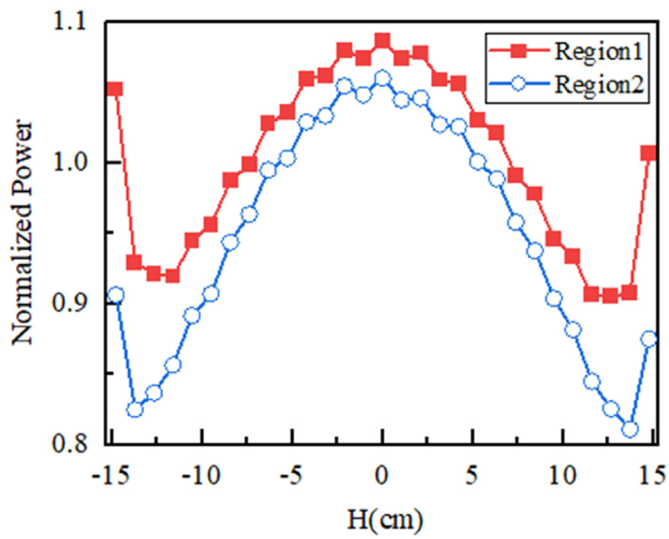

Fig. 9. Power variation along the axial direction in region 1 and region 2.

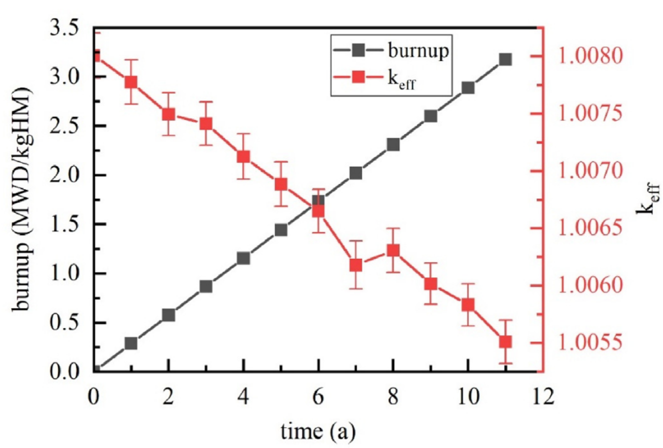

Fig. 10. k_{eff} and burnup versus time.

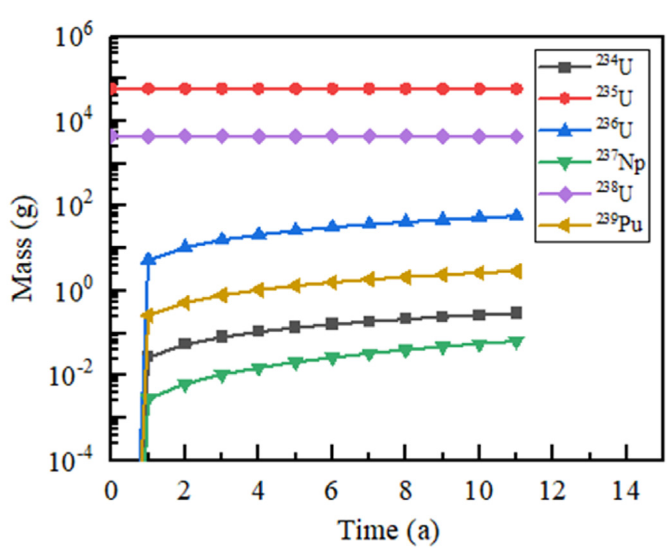

Fig. 11. Changes in main heavy metal composition.

thermal conductivity of the heat pipe. The calculation results under the two conditions are compared in the supplementary materials, and the temperature and velocity distributions are not significantly different. In this subsection, the heat pipe is set as a constant temperature wall, and the flow and heat transfer characteristics of D^2-SMSR are studied under the gravity environment of Mars ($g = 3.6\ m/s^2$).

4.2.1. Temperature field distribution

The temperature distribution of the core is shown in Fig. 12. Natural convection causes hot fluid to move upward and cold fluid to move downward, causing an obvious thermal stratification at the core. Fig. 13 shows the radial distribution of temperature in the two symmetrical sections. The gray bars represent the position of the heat pipe, and the black bars represent the part of the alloy coating the fuel. Given the heat absorption of the heat pipes, the heat uniformity along the radial direction is enhanced. The core temperatures are less uniform near the top and bottom than those in the middle. The average temperature in region 2 is approximately 20 K higher than that in region 1. The average heat transfer coefficient h_{ave} is defined as follows:

$$h_{ave} = \frac{q_{ave}}{T_{ave} - T_{cold}}$$

where q_{ave} is the heat flux (W/m^2), T_{ave} is the average temperature of the core, and T_{cold} is the temperature of the cold source. According to the calculated result, $h_{ave} = 1.33\ kW\ m^{-2}\ K^{-1}$.

4.2.2. Flow field structural variation

Fig. 14 shows the velocity distribution in the D^2-SMSR. The velocity distribution in the core is concentrated near the heat pipe and in the middle of the core. A certain velocity distribution is observed on the wall between region 1 and region 2. Region 1 has a higher velocity flow near the bottom of the core, which can be

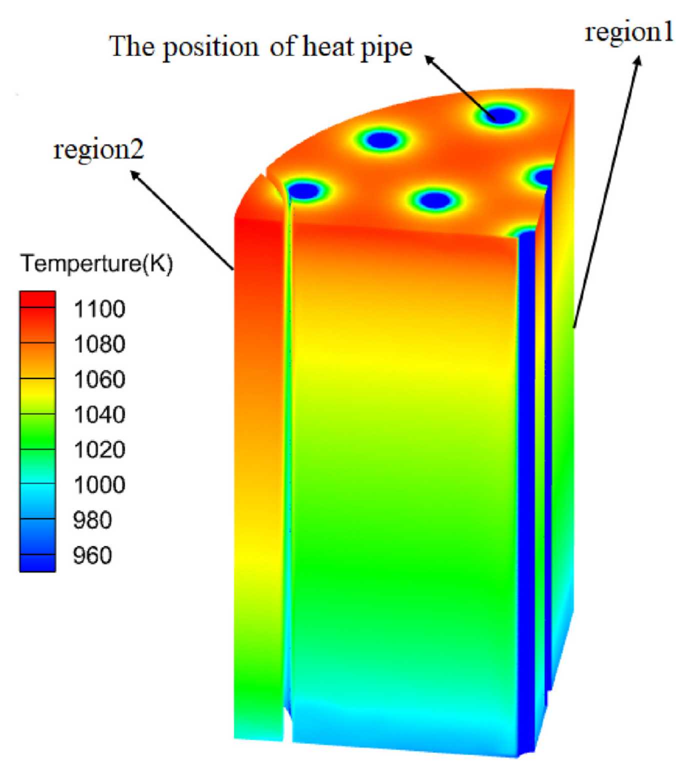

Fig. 12. Contour of temperature distribution of the 1/4 core.

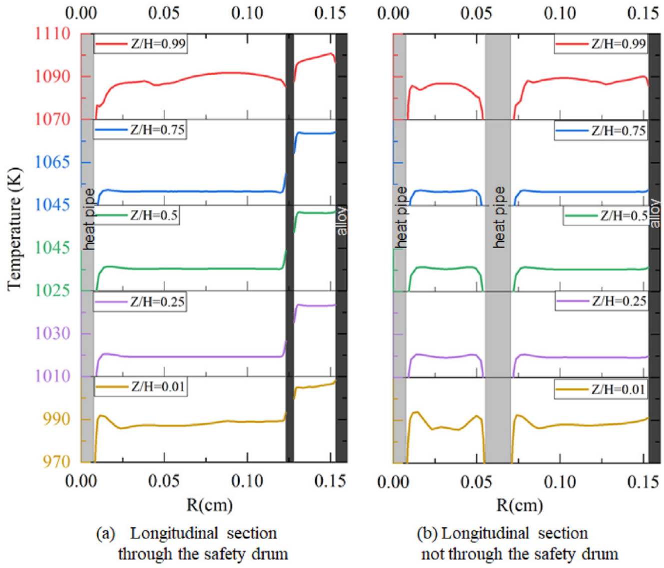

Fig. 13. Temperature plots for different heights and radial positions.

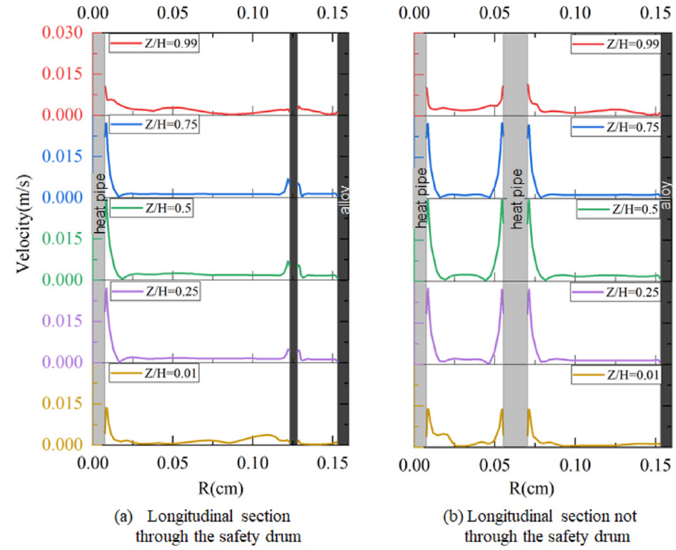

Fig. 15. Velocity distribution at different heights and radial positions.

explained by the temperature difference between the two fission regions. In addition, the temperature difference aggravates the natural convection effect of the liquid molten salt. This effect is more obvious at the bottom of the core, leading to a higher velocity near the safety drum at the bottom. Fig. 14(a) and (c) show the downward flow near the alloy occur only in region 2, but not in region 1. This phenomenon is related to the convection in region 1 and region 2. As shown in Fig. 13 (a), at the same height, the temperature of region 2, region 1 and the alloy between them is $T_{r2}>T_{alloy}>T_{r1}$. For region 2, the alloy is a cold wall. The fluid density near it is large and sinks, and the flow direction is downward. While for region 1, the alloy is a hot wall. The fluid density near it is small and floating upward, and the flow direction is upward. Fig. 15 shows the radial velocity distribution in the two symmetrical sections. The positions with high velocity are all near the wall of the heat pipe, corresponding to the parts with a large temperature gradient.

4.2.3. *Influence of heat pipe position*

Different depths of heat pipes inserted into the core affect the reactor's flow and heat transfer characteristics. On the one hand, the deeper the insertion of heat pipes, the larger the contact wall with the core and the larger the heat transfer area, which is beneficial for heat transfer. On the other hand, maintaining a certain distance between the heat pipe and the bottom strengthens the local convection in the core [36]. As a result, the liquid molten salt becomes more fluid and promotes convective heat transfer in the reactor. The temperature and velocity of two cases are

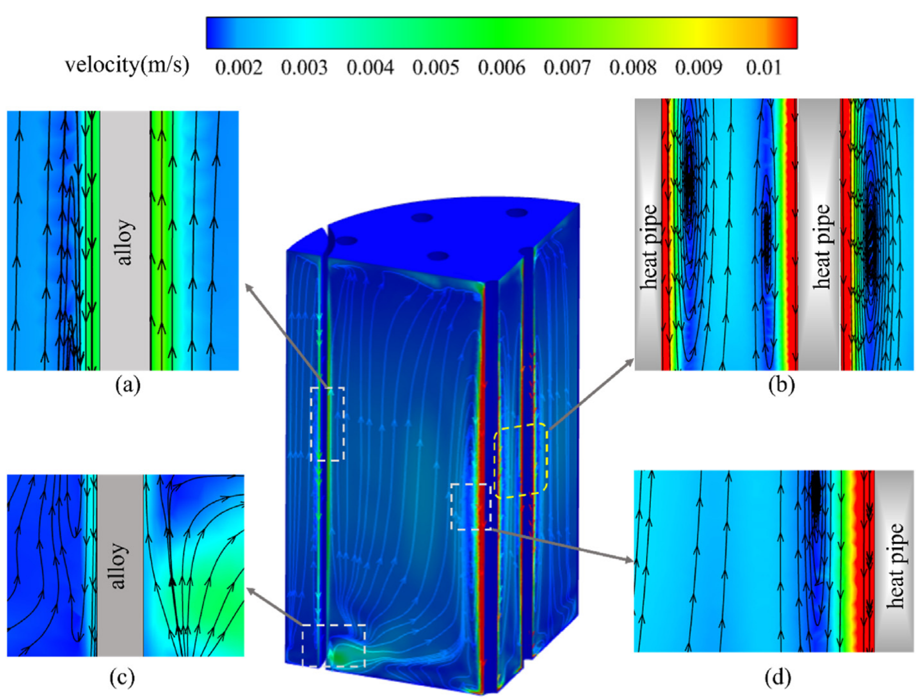

Fig. 14. Contour of the velocity distribution of the 1/4 core.

compared to explore the influence of different heat pipe insertion depths on flow and heat transfer characteristics.

As shown in Figs. 16 and 17, when the heat pipe is at a certain distance from the bottom of the core (h = 0.05 H), the heat transfer area at the bottom decreases. However, the convection effect in the local area at the bottom of the heat pipe is strengthened, and the fluidity of molten salt is enhanced. This situation causes a slightly smooth change in the temperature in the middle area. Although the average temperature is higher when h = 0.05 H, the average heat transfer coefficient h_{ave} is 1.39 kW m^{-2} K^{-1}, which is greater than the value of h = 0 (1.33 kW m^{-2} K^{-1}), indicating a better heat transfer performance.

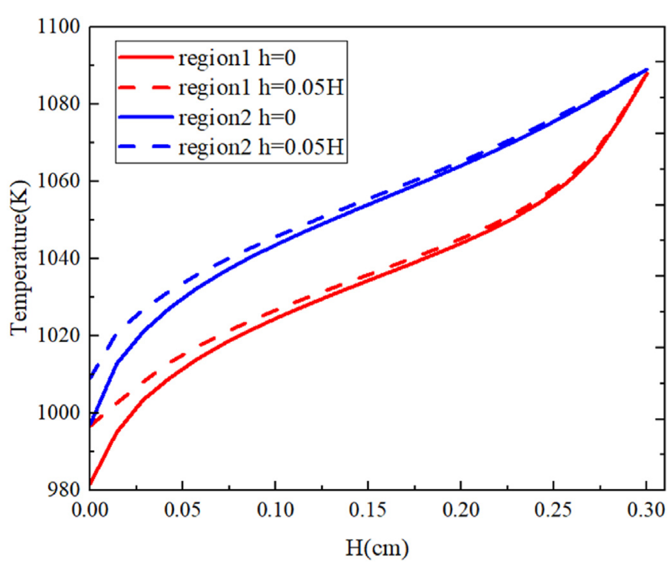

Fig. 16. Temperature distribution along the height direction in region 1 and region 2.

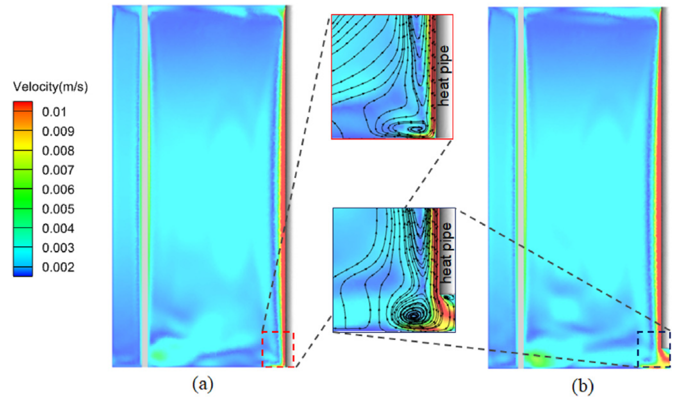

Fig. 17. Effects of different heat pipe insertion depths on velocity distributions ((a): heat pipe contact with the bottom of the core; (b): heat pipe is 0.05 H from the bottom of the core).

4.3. Dual drum value analysis of D^2-SMSR

Safety drums and control drums regulate the reactivity of D^2-SMSR. Control drums are used during a regular operation to control reactivity. Safety drums are used to shut down the core in an emergency. A discussion of the regulation effect of control drums on reactivity and the safe shutdown capability of the reactor under partial drum failure is presented in this subsection.

4.3.1. Reactivity control analysis

Fig. 18 shows the variation of k_{eff} when the working temperature is from 773 K (melting point temperature of molten salt) to 1000 K (operating temperature). The effective multiplication factor k_{eff} decreases linearly with the increase in temperature. The average reactivity temperature coefficient is calculated as

$$\alpha_T = \frac{\frac{1}{k_{eff1}} - \frac{1}{k_{eff2}}}{T_2 - T_1}$$

where α_T is the reactivity temperature coefficient of reactor core, and k_{eff1} (or k_{eff2}) is the effective multiplication factor when the temperature is T_1 (or T_2). According to the calculated result, α_T = -4.85 pcm/K. As can be seen from Table 2, D^2-SMSR has a slightly large negative feedback temperature coefficient and high inherent safety.

For a molten salt reactor, temperature affects the reaction cross-section between the core material and neutrons, eventually changing reactivity. The temperature also affects the density of molten salt, further affecting the reactivity. Fig. 18 shows the influence of the two changes. Liquid fuel is primarily responsible for the reactivity change in the D^2-SMSR. Table 3 gives the total reactivity of materials temperature (excluding the reactivity caused by fuel density). For D^2-SMSR, the influence of core material temperature on the reactivity coefficient mainly lies in the temperature of the reflector. The reactivity coefficient caused by material temperature is negative, and the reactivity caused by fuel density is positive. The reactivity change caused by density is far greater than that caused by core material temperature, which finally causes the reactor to have a negative feedback coefficient.

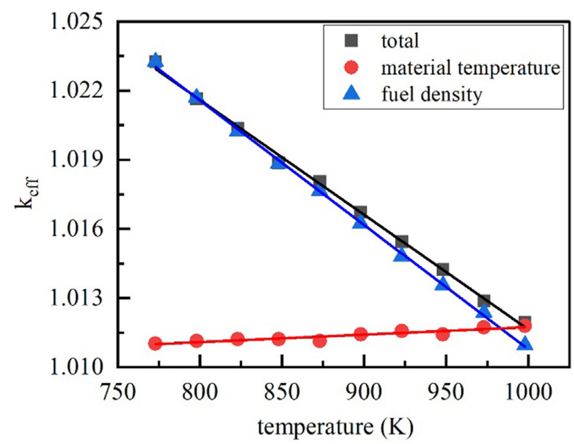

Fig. 18. Influence of temperature on reactivity.

This study calculates a variation in the k_{eff} with the angle of the control drum at T = 773 K and T = 1000 K to investigate the effect of control drum rotation on reactivity. As stipulated, the rotation angle is 0° when the absorber of the control drum is closest to the core and 180° when it is farthest from the core. The results are shown in

Table 2
Comparison of reactivity temperature coefficients of different reactor types.

Reactor name	Reactivity temperature coefficients (pcm/K)
KRUSTY	-0.77 [37].
SNCLFR-100	-1.27 [38].
PWR[a]	-5~-2
D^2-SMSR	-4.85

[a] For pressurized water reactor, only the fuel temperature coefficient is concerned.

Table 3
Temperature coefficient of core material.

Reflector	Fuel Doppler effect	Total
0.40 pcm/K	-0.08 pcm/K	0.33 pcm/K

Fig. 19. With the increase in the rotation angle of the control drum, the effective multiplication factor increases non-linearly. The reactivity value of the control drums at T = 773 K is 5128 pcm; at T = 1000 K, it is 5481 pcm. The findings suggest that when the reactor is shut down at the working temperature, the temperature of the core drops, leading to a slight reduction in the shutdown margin. In addition, when the spacecraft falls in a launch accident, the reactor may suffer from water flooding or sand flooding. This situation moderates the neutrons in the core and causes a sharp increase in reactivity. In this case, the reactor may return to criticality. Therefore, $k_{eff} < 0.98$ should be considered in the shutdown state to ensure the shutdown safety of the space nuclear reactor [39]. The D^2-SMSR has sufficient margin to ensure shutdown in case of an accident.

4.3.2. Shutdown strategy analysis

The reactivity of the D^2-SMSR is controlled by four control drums and two safety drums, as shown in Fig. 20. The worth of control drums and safety drums is shown in Fig. 21. With the change of angle, the effect of two safety drums on k_{eff} of the core is greater than that of four control drums, with a deeper shutdown margin. This result means that the safety drum can reduce core reactivity more quickly. Subsequently, the changes in reactivity during certain control drums and safety drums failures are analyzed. According to calculations, k_{eff} of the shutdown is 0.97397 when a single safety drum is working, and it is 0.97045 when three control drums are working, as shown in Table 4. Therefore, a single safety drum or three control drums can realize the normal shutdown of the reactor.

5. Conclusion

This study has proposed a conceptual design of the D^2-SMSR. The molten salt LiF–UF_4 served as fuel with heat pipes exhausting the released heat. Control drums and safety drums are used for reactivity control and emergency shutdown. Critical characteristics of neutron physics and thermal hydraulics are determined. The conclusions of this study can be summarized as follows:

(1) The D^2-SMSR has a fast neutron energy spectrum with a temperature coefficient of -4.85 pcm/K, which can meet the 10-year life requirement at the full power of 40 kWth.
(2) The natural convection flow of molten salt in D^2-SMSR can enhance core's flow and improve core's heat transfer effect.

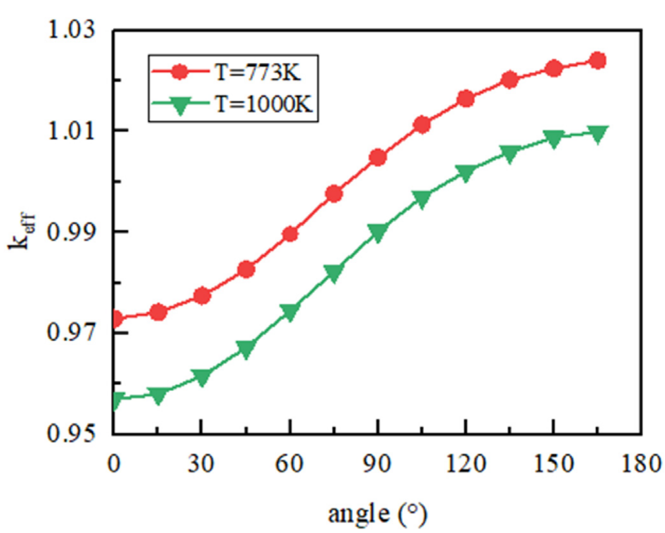

Fig. 19. Effect of control drum rotation angle on reactivity.

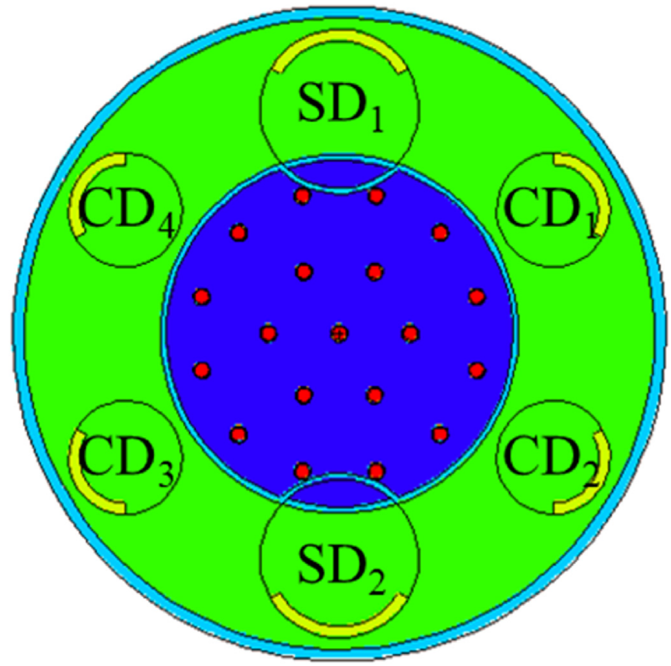

Fig. 20. Distribution of safety drums (SDs) and control drums (CDs).

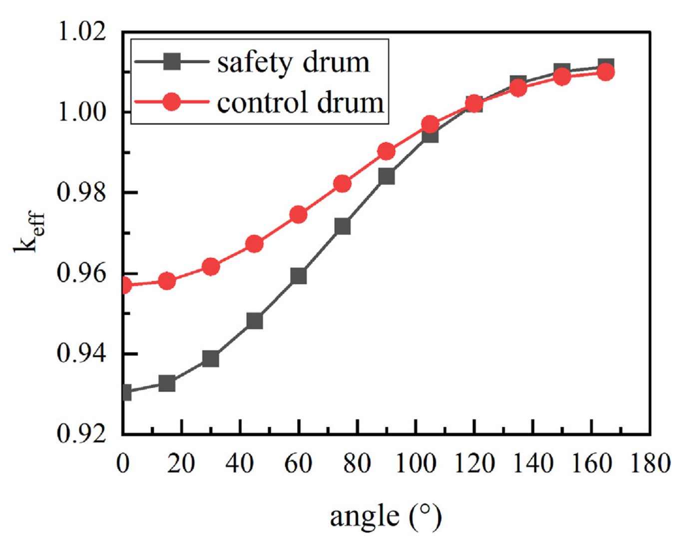

Fig. 21. Effect of control drums and safety drums on reactivity.

Table 4
k_{eff} versus control (safety) drum failure position and number.

Failure position	k_{eff}
SD_1(or SD_2)	0.97397
CD_1	0.97045
CD_1 and CD_2	0.98503
CD_1 and CD_3	0.98390
CD_1 and CD_4	0.98390

The heat transfer performance is strengthened when the bottom distance between the heat pipes and reactor core is 0.05H.

(3) The new nuclear safety strategy of combining control drums and safety drums can achieve higher safety standards, and only a single safety drum or three control drums are needed for normal shutdown.

Declaration of competing interest

The authors declare that they have no known competing financial interests or personal relationships that could have appeared to influence the work reported in this paper.

Acknowledgments

This work was supported by the National Natural Science Foundation of China (Grant Nos. 12105142 and 12205152), the Jiangsu Planned Projects for Postdoctoral Research Funds (Grant No. 2021K387C) and the Natural Science Foundation of Jiangsu Province (Grant No. BK20220904).

Appendix A. Supplementary data

Supplementary data to this article can be found online at https://doi.org/10.1016/j.net.2023.03.011.

References

[1] L. Watson-Morgan, G. Chavers, J. Connolly, K. Crowe, D. Krupp, L. Means, T. Percy, T. Polsgrove, J. Turpin, NASA's initial and sustained artemis human landing systems, IEEE Aerosp. Conf. 50100 (2021) 1–11, https://doi.org/10.1109/AERO50100.2021.9438179, 2021.

[2] R. Verduci, V. Romano, G. Brunetti, N. Yaghoobi Nia, A. Di Carlo, G. D'Angelo, C. Ciminelli, Solar energy in space applications: review and technology perspectives, Adv. Energy Mater. 12 (2022), 2200125, https://doi.org/10.1002/aenm.202200125.

[3] N. Lior, Power from space, Energy Convers. Manag. 42 (2001) 1769–1805, https://doi.org/10.1016/S0196-8904(01)00040-1.

[4] B. Heshmatpour, A. Lieberman, M. Khayat, A. Leanna, T. Dobry, Special application thermoelectric micro isotope power sources, AIP Conf. Proc. 969 (2008) 689–695, https://doi.org/10.1063/1.2845032.

[5] R.C. O'Brien, R.M. Ambrosi, N.P. Bannister, S.D. Howe, H.V. Atkinson, Safe radioisotope thermoelectric generators and heat sources for space applications, J. Nucl. Mater. 377 (2008) 506–521, https://doi.org/10.1016/j.jnucmat.2008.04.009.

[6] G. Bennett, Space nuclear power: opening the final frontier, in: 4th Int. Energy Convers. Eng. Conf. Exhib. IECEC, American Institute of Aeronautics and Astronautics, San Diego, California, 2006, https://doi.org/10.2514/6.2006-4191.

[7] Zhiwen Dai, Chenglong Wang, Dalin Zhang, Wenxi Tian, Suizheng Qiu, G.H. Su, Numerical simulation on thermal-hydraulic and thermoelectric characteristics of the TOPAZ-II reactor core, Int. J. Energy Res. 45 (2021) 12159–12172, https://doi.org/10.1002/er.6170.

[8] M. Kambe, H. Tsunoda, K. Mishima, T. Iwamura, Rapid-L operator-free fast reactor concept without any control rods, Nucl. Technol. 143 (2003) 11–21, https://doi.org/10.13182/NT03-A3394.

[9] L. Mason, D. Poston, L. Qualls, System Concepts for Affordable Fission Surface Power, 2008. https://ntrs.nasa.gov/citations/20080013229.

[10] J.C. King, M.S. El-Genk, Submersion-subcritical safe space (S4) reactor, Nucl. Eng. Des. 236 (2006) 1759–1777, https://doi.org/10.1016/j.nucengdes.2005.12.010.

[11] T. Meng, K. Cheng, C. Zeng, Y. He, S. Tan, Preliminary control strategies of megawatt-class gas-cooled space nuclear reactor with different control rod configurations, Prog. Nucl. Energy 113 (2019) 135–144, https://doi.org/10.1016/j.pnucene.2019.01.013.

[12] D.I. Poston, The heatpipe-operated Mars exploration reactor (HOMER), in: AIP Conf. Proc., AIP, Albuquerque, New Mexico, 2001, pp. 797–804, https://doi.org/10.1063/1.1358010.

[13] Y. Ma, M. Liu, B. Xie, W. Han, X. Chai, S. Huang, H. Yu, Neutronic and thermal-mechanical coupling schemes for heat pipe-cooled reactor designs, J. Nucl. Eng. Radiat. Sci. 8 (2022), 021303, https://doi.org/10.1115/1.4051612.

[14] D.I. Poston, M. Gibson, P. McClure, KILOPOWER REACTORS FOR POTENTIAL SPACE EXPLORATION MISSIONS, in: NETS-2019-Pap, 2019, p. 6. Richland, WA, http://anstd.ans.org/.

[15] P.N. Haubenreich, J.R. Engel, Experience with the molten-salt reactor experiment, Nucl. Appl. Technol. 8 (1970) 118–136, https://doi.org/10.13182/NT8-2-118.

[16] L. Mathieu, D. Heuer, R. Brissot, C. Garzenne, C. Le Brun, D. Lecarpentier, E. Liatard, J.-M. Loiseaux, O. Méplan, E. Merle-Lucotte, A. Nuttin, E. Walle, J. Wilson, The thorium molten salt reactor: moving on from the MSBR, Prog. Nucl. Energy 48 (2006) 664–679, https://doi.org/10.1016/j.pnucene.2006.07.005.

[17] D. Zhang, L. Liu, M. Liu, R. Xu, C. Gong, J. Zhang, C. Wang, S. Qiu, G. Su, Review of conceptual design and fundamental research of molten salt reactors in China, Int. J. Energy Res. 42 (2018) 1834–1848, https://doi.org/10.1002/er.3979.

[18] S. Greene, J. Gehin, D. Holcomb, J. Carbajo, D. Ilas, A. Cisneros, V. Varma, W. Corwin, D. Wilson, G. Yoder, A. Qualls, F. Peretz, G. Flanagan, D. Clayton, E. Bradley, G. Bell, J. Hunn, P. Pappano, S. Cetiner, Pre-Conceptual Design of a Fluoride-Salt-Cooled Small Modular Advanced High Temperature Reactor, SmAHTR), 2011, https://doi.org/10.2172/1008830.

[19] A. Rykhlevskii, B.R. Betzler, A. Worrall, K.D. Huff, Fuel Cycle Performance of Fast Spectrum Molten Salt Reactor Designs, Oak Ridge National Lab. (ORNL), Oak Ridge, TN (United States), 2019, https://doi.org/10.31224/osf.io/zkvn9.

[20] Rei Kimura, Tadashi Yoshida, Design study of molten-salt-type reactor for powering space probes and its automated start-up, J. Nucl. Sci. Technol. 50 (2013) 998–1010, https://doi.org/10.1080/00223131.2013.829284.

[21] M. Eades, J. Flanders, N. McMurray, R. Denning, X. Sun, W. Windl, T. Blue, Space molten salt reactor concept for nuclear electric propulsion and surface power, J. Br. Interplanet. Soc. 64 (2011) 186–193.

[22] L. Ting, Z. Kun, S. Wen, T. Xiaobin, Preliminary neutronics design of space nuclear reactor based on molten salt cooling, Nucl. Tech. 43 (2020) 34–42 (in Chinese).

[23] D.Y. Cui, Y. Dai, X.Z. Cai, Y. Fu, X.X. Li, Y. Zou, J.G. Chen, Preconceptual nuclear design of a 50 kWth heat pipe cooled micro molten salt reactor (micro-MSR), Prog. Nucl. Energy 134 (2021), 103670, https://doi.org/10.1016/j.pnucene.2021.103670.

[24] Y. Shihe, S. Qiang, Z. Heng, Y. Rui, Z. Yang, L. Bing, Conceptual design of Mars molten salt reactor, Nucl. Tech. 43 (2020) 67–72 (in Chinese).

[25] J. Serp, M. Allibert, O. Beneš, S. Delpech, O. Feynberg, V. Ghetta, D. Heuer, D. Holcomb, V. Ignatiev, J.L. Kloosterman, L. Luzzi, E. Merle-Lucotte, J. Uhlíř, R. Yoshioka, D. Zhimin, The molten salt reactor (MSR) in generation IV: overview and perspectives, Prog. Nucl. Energy 77 (2014) 308–319, https://doi.org/10.1016/j.pnucene.2014.02.014.

[26] D. LeBlanc, Molten salt reactors: a new beginning for an old idea, Nucl. Eng. Des. 240 (2010) 1644–1656, https://doi.org/10.1016/j.nucengdes.2009.12.033.

[27] L. Mathieu, D. Heuer, E. Merle-Lucotte, R. Brissot, C. Le Brun, E. Liatard, J.-M. Loiseaux, O. Méplan, A. Nuttin, D. Lecarpentier, Possible configurations for the thorium molten salt reactor and advantages of the fast nonmoderated version, Nucl. Sci. Eng. 161 (2009) 78–89, https://doi.org/10.13182/NSE07-49.

[28] B.M. Elsheikh, Safety assessment of molten salt reactors in comparison with light water reactors, J. Radiat. Res. Appl. Sci. 6 (2013) 63–70, https://doi.org/10.1016/j.jrras.2013.10.008.

[29] T.M. Schriener, M.S. El-Genk, Reactivity control options of space nuclear reactors, Prog. Nucl. Energy 51 (2009) 526–542, https://doi.org/10.1016/j.pnucene.2008.11.003.

[30] A.E. Craft, J.C. King, Reactivity control schemes for fast spectrum space nuclear reactors, Nucl. Eng. Des. 241 (2011) 1516–1528, https://doi.org/10.1016/j.nucengdes.2011.01.049.

[31] H.C. Lee, T.Y. Han, H.S. Lim, J.M. Noh, An accident-tolerant control drum system for a small space reactor, Ann. Nucl. Energy 79 (2015) 143–151, https://doi.org/10.1016/j.anucene.2015.02.001.

[32] M.A. Gibson, D.I. Poston, P.R. McClure, J.L. Sanzi, T.J. Godfroy, M.H. Briggs, S.D. Wilson, N.A. Schifer, M.F. Chaiken, N. Lugasy, Heat transport and power conversion of the kilopower reactor test, Nucl. Technol. 206 (2020) 31–42, https://doi.org/10.1080/00295450.2019.1709364.

[33] L. Dewan, Molecular Dynamics Simulation and Topological Analysis of the Network Structure of Actinide-Bearing Materials, Thesis, Massachusetts Institute of Technology, 2013. https://dspace.mit.edu/handle/1721.1/86266.

[34] K. Wang, Z. Li, D. She, J. Liang, Q. Xu, Y. Qiu, J. Yu, J. Sun, X. Fan, G. Yu, RMC – a Monte Carlo code for reactor core analysis, Ann. Nucl. Energy 82 (2015) 121–129, https://doi.org/10.1016/j.anucene.2014.08.048.

[35] F.G. Schmitt, About Boussinesq's turbulent viscosity hypothesis: historical remarks and a direct evaluation of its validity, Comptes Rendus Mécanique 335 (2007) 617–627, https://doi.org/10.1016/j.crme.2007.08.004.

[36] L. Zhang, J. Deng, W. Sun, Z. Ma, G.H. Su, L. Pan, Performance analysis of natural convection in presence of internal heating, strong turbulence and phase change, Appl. Therm. Eng. 178 (2020), 115602, https://doi.org/10.1016/j.applthermaleng.2020.115602.

[37] D.I. Poston, M.A. Gibson, T.J. Godfroy, P.R. McClure, KRUSTY reactor design, Nucl. Technol. 206 (2020) 13–30, https://doi.org/10.1080/00295450.2020.1725382.

[38] H. Chen, Z. Chen, C. Chen, X. Zhang, H. Zhang, P. Zhao, K. Shi, S. Li, J. Feng, Q. Zeng, Conceptual design of a small modular natural circulation lead cooled fast reactor SNCLFR-100, Int. J. Hydrogen Energy 41 (2016) 7158–7168, https://doi.org/10.1016/j.ijhydene.2016.01.101.

[39] J.C. King, M.S. El-Genk, Temperature and burnup reactivities and operational lifetime for the submersion-subcritical, safe space (S^4) reactor, Nucl. Eng. Des. 237 (2007) 552–564, https://doi.org/10.1016/j.nucengdes.2006.07.008.